Supporting Information

PVP-Stabilized Intermediates Promote C-C Coupling for Selective CO_2 Electroreduction to C_{2+} Products on CuO Catalysts

Fucang Liang, Xueyan Wu, Penggao Liu, Yan Lv*, Jixi Guo*

State Key Laboratory of Chemistry and Utilization of Carbon-Based Energy Resources;

College of Chemistry, Xinjiang University, Urumqi, 830017, Xinjiang, P.R. China.

E-mail: lvyan2014@xju.edu.cn; jxguo1012@163.com.

Quantitative analysis of products

The gas products were detected and analyzed using online gas chromatography (FULI INSTRUMENTS GC 9790II). A thermal conductivity detector (TCD) measured the amount of H_2 produced, while a flame ionization detector (FID) measured the quantities of CO, CH_4, and C_2H_4 generated. The FEs were calculated by：

$$\text{FE}\ (\%) = \frac{V \times Q \times P \times nF}{R \times T \times i} \times 100\%$$

where V is the volume concentration fom GO, i is the current recorded. by the workstation, P is pressure, F is the Faradaic constant, 96485 C mo^{-1}, R is the ideal gas constant, 8.314 m^3. Pa (K·mol), Q is fow rate, 23 ml, min^{-1}, and T is temperature.

After a constant potential reaction, the liquid products were sampled with a syringe, and 600 μl of the collected electrolyte was mixed with 100 μl of D_2O (deuterated water) and 100 μl of DMSO (dimethyl sulfoxide, internal standard) for analysis using ^1H nuclear magnetic resonance (^1H-NMR AVANCE NEO600). The ^1H–NMR spectrum was measured with water suppression using a pre-saturation method. The quantification was achieved by internal standard method with an internal standard aqueous solution of 50 dimethyl sulfoxide. The FE for the products were calculated as follows:

$$\text{FE}\ (\%) = \frac{C \times V \times nF}{Q} \times 100\%$$

where Concentration (C) was obtained from NMR, V is clectrolyte volume, F is the Faradaic constant, Q is the electricity record by the workstation.

It is worth noting that the test results of all gas and liquid products are the average

of the three tests.

The calculation methods of CO conversion rate and H–content in products are shown in the following:

CO conversion rate:

$$= \frac{n_{CH4} + 2n_{C2H4} + 2n_{CH3CH2OH} + 3n_{CH3CH2CH2OH}}{n_{CO} + n_{CH4} + 2n_{C2H4} + 2n_{CH3CH2OH} + 3n_{CH3CH2CH2OH}}$$

Where n_x is the mole of product, which can be obtained from GC or 1H NMR.

H-content in products:

$$= \frac{2 \times FE_{H2}}{2} + \frac{4 \times FE_{CH4}}{8} + \frac{2 \times FE_{HCOOH}}{2} + \frac{4 \times FE_{C2H4}}{12} + \frac{6 \times FE_{CH3CH2OH}}{12} + \frac{8 \times FE_{CH3CH2CH2OH}}{18}$$

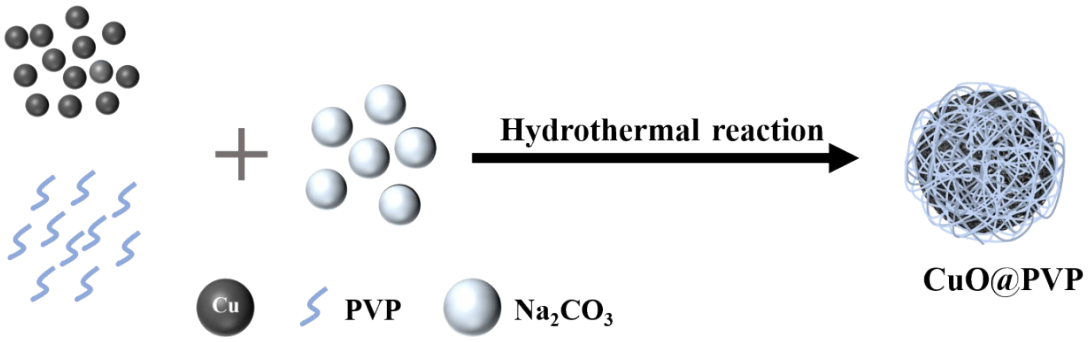

Figure S1. The synthetic process of CuO@PVP.

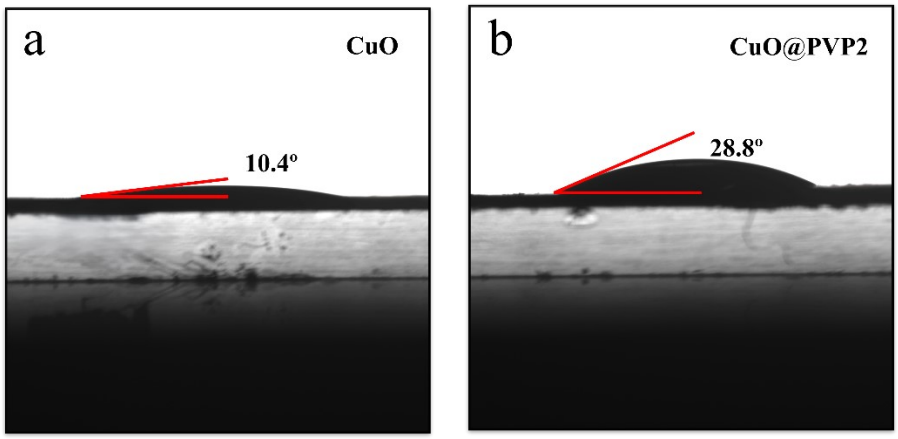

Figure S2. Photographs of contact angle measurements on the (a) CuO and (b) CuO@PVP.

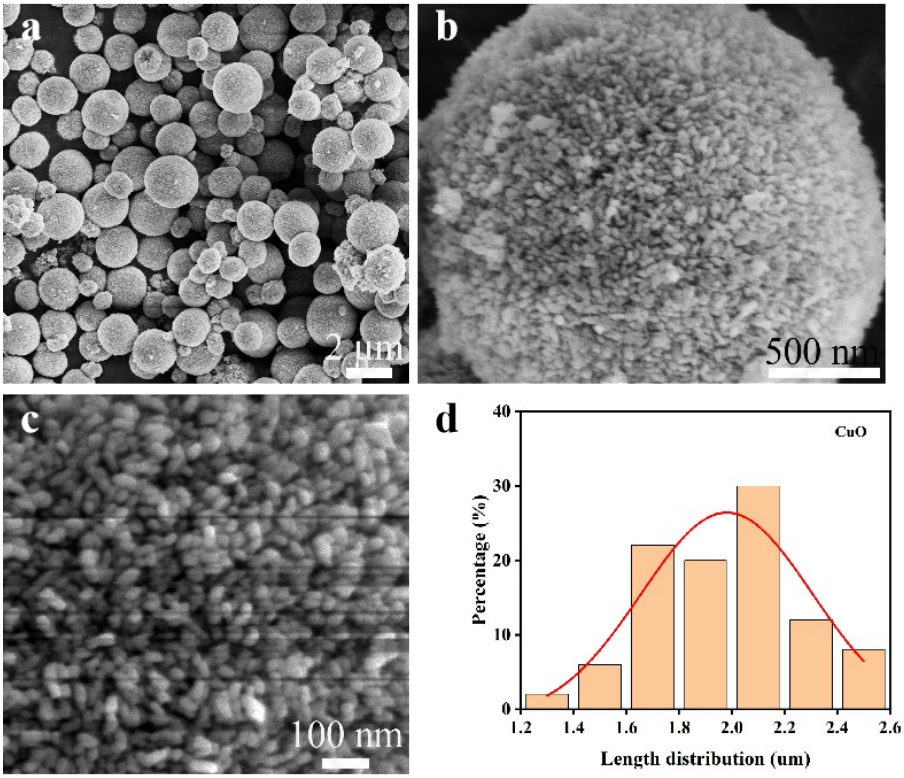

Figure S3. (a-c) SEM images of the CuO, and (d) particle size distribution of CuO.

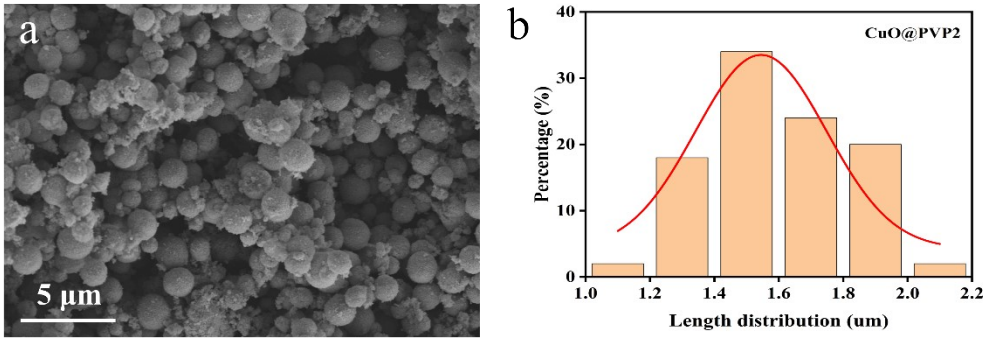

Figure S4. (a) SEM images of the CuO@PVP2, and (b) particle size distribution of CuO.

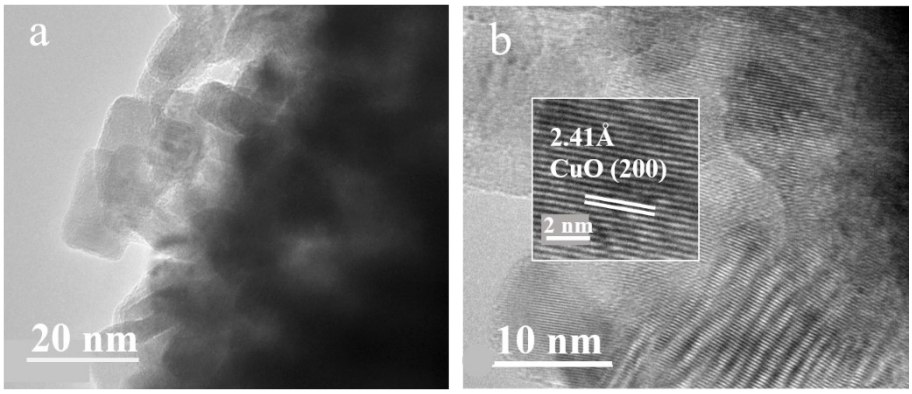

Figure S5. (a-b) The TEM images of CuO.

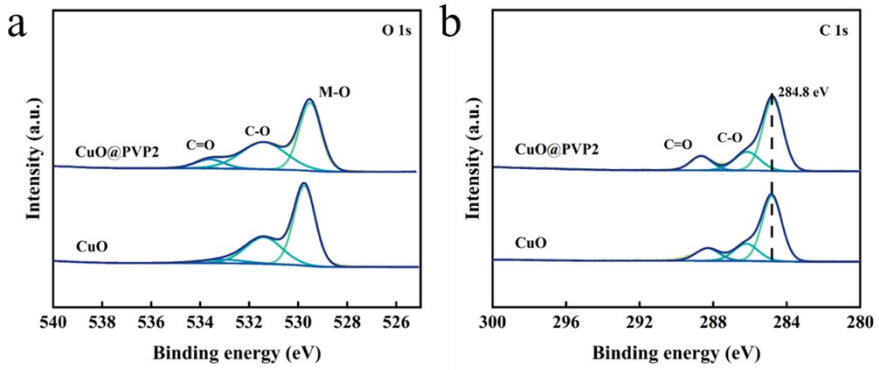

Figure S6. (a) O 1s and C 1s XPS patterns of CuO and CuO@PVP2.

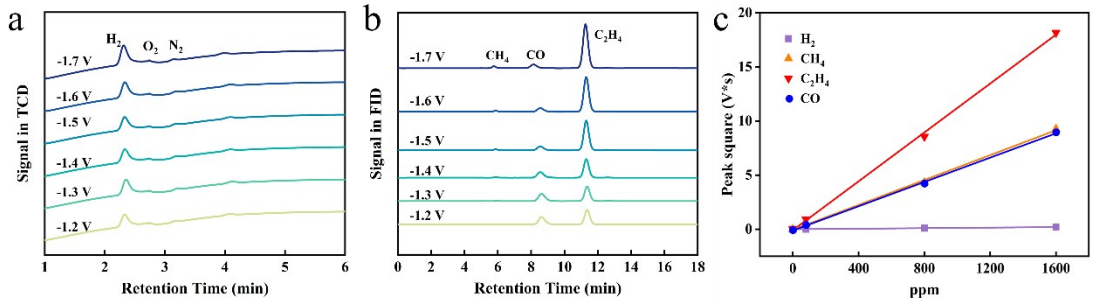

Figure S7. In-stiu-gas-chromatography spectra under various potentials of CuO@PVP2 in chronoamperometry detected by (a) FID and (b) TCD detectors; (c) Standard curve.

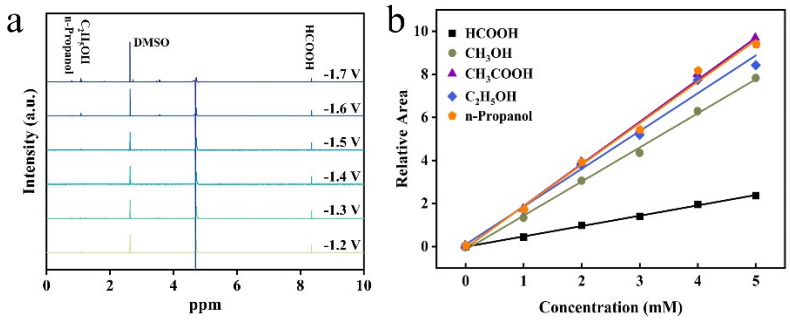

Figure S8. ^{1}H-NMR spectra under various potentials of CuO@PVP2 in chronoamperometry; (b) Standard curve.

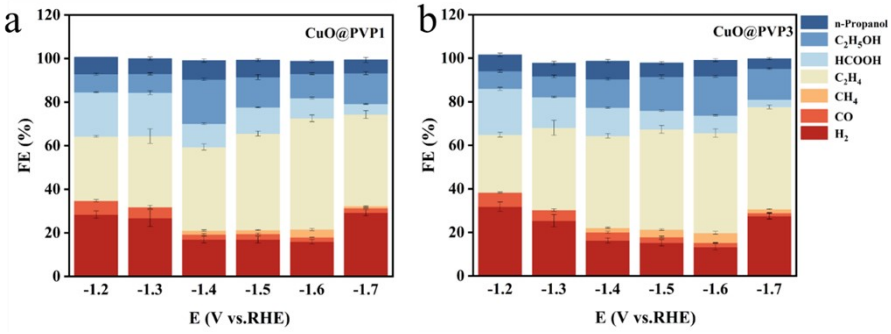

Figure S9. The FE for each CO_2RR product on (a) CuO@PVP1 and (b) CuO@PVP3.

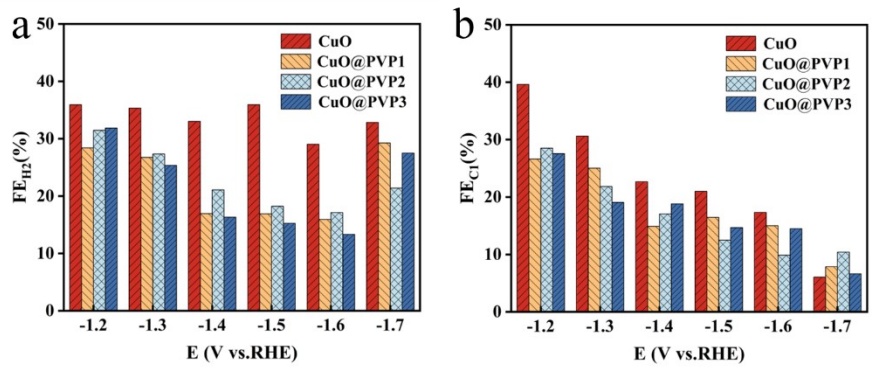

Figure S10. CuO, CuO@PVP1, CuO@PVP2, and CuO@PVP3 at various potentials: (a) FE_{H2} and (b) FE_{C1}.

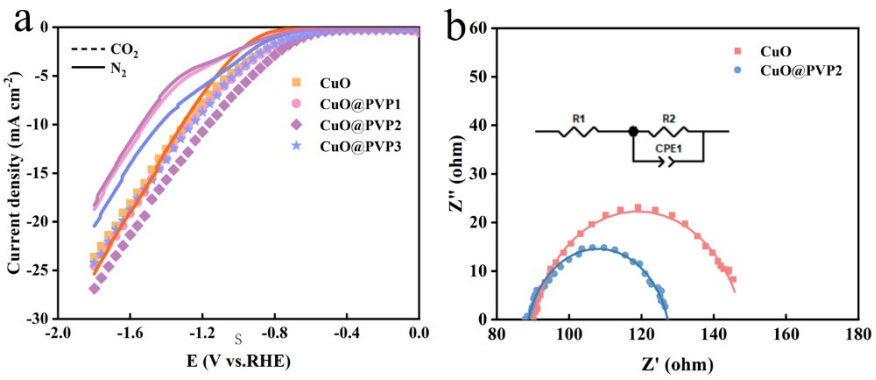

Figure S11. (a) LSV curves of CuO, CuO@PVP1, CuO@PVP2, and CuO@PVP3 under N_2 and CO_2 atmospheres, (b) EIS spectra of CuO and CuO@PVP2 at –1.5 V (vs. RHE).

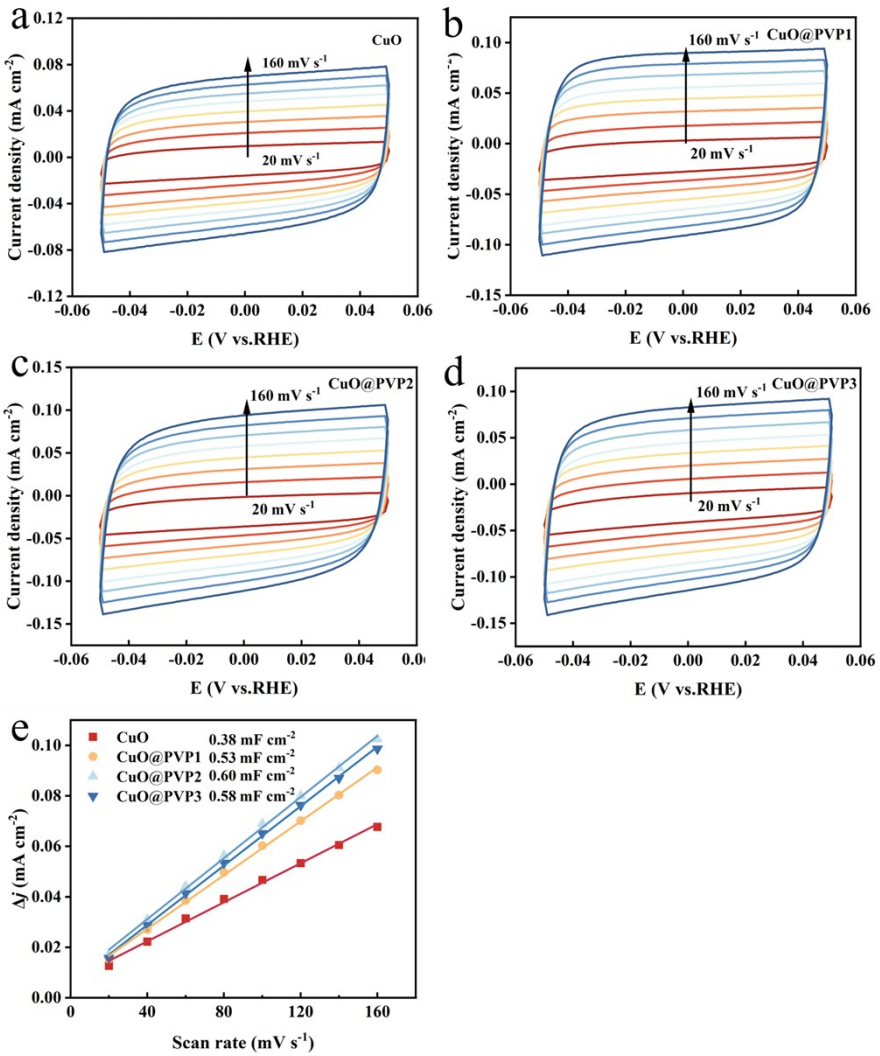

Figure S12. C_{dl} of CuO, CuO@PVP1, CuO@PVP2 and CuO@PVP3 catalysts. (a–d) CV curves at different scan rates. (e) Plot of difference in charging current density vs. scan rate.

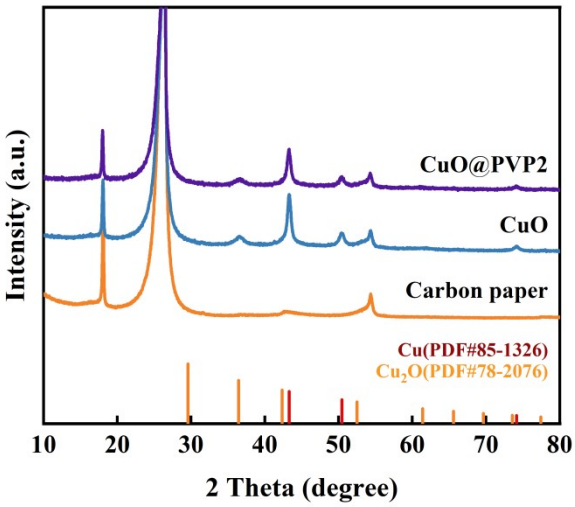

Figure S13. XRD patterns CuO@PVP2 and CuO after CO_2 electroreduction.

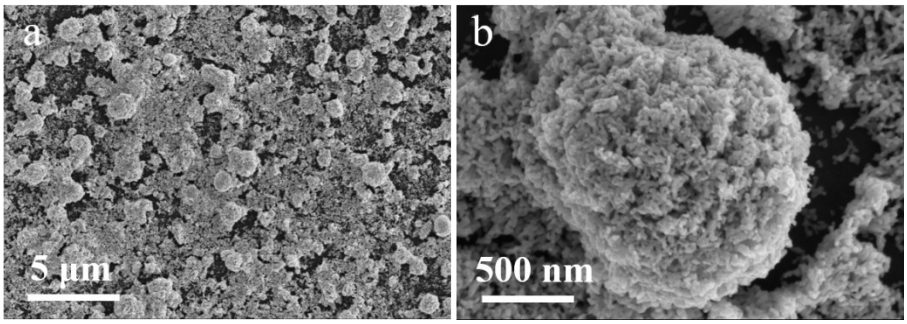

Figure S14. (a-b) SEM images of the CuO sample after electroreduction.

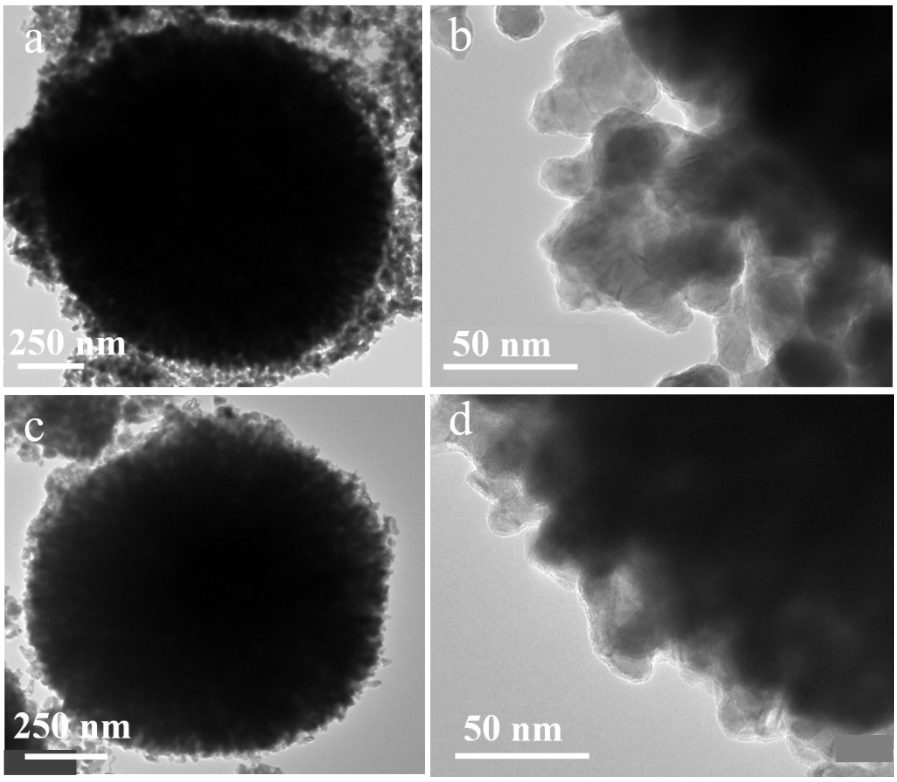

Figure S15. TEM images of the (a-b) CuO sample (c-d) CuO@PVP2 after electroreduction.

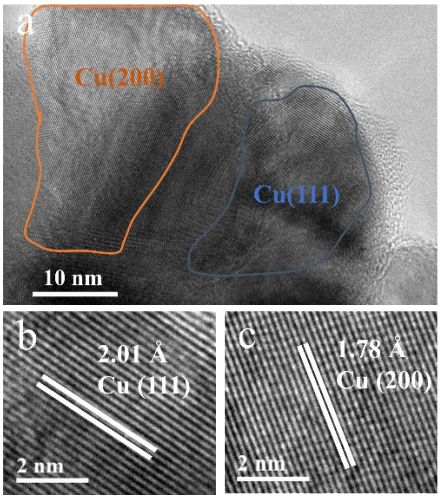

Figure S16. (a) HRTEM images of the CuO. (b) Lattice fringes correspond to the blue region. (c) Lattice fringes corresponding to the orange region.

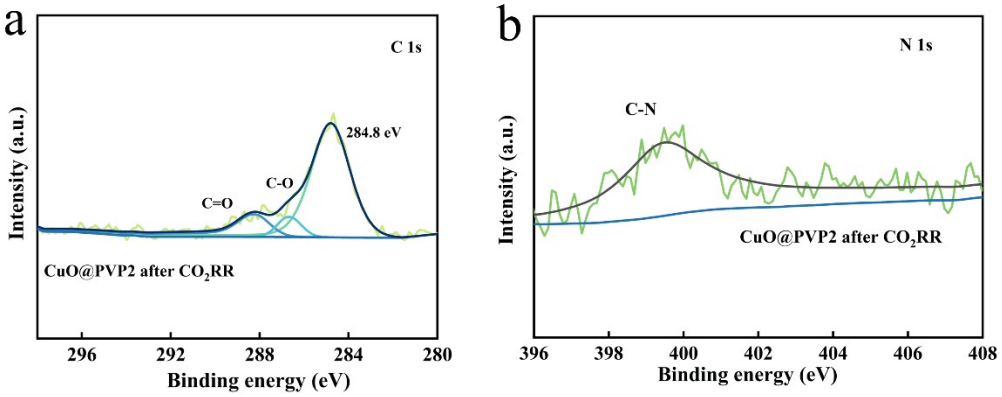

Figure S17. XPS images of (a) C 1s and (b) N 1s of the CuO@PVP2 catalyst after electroreduction.

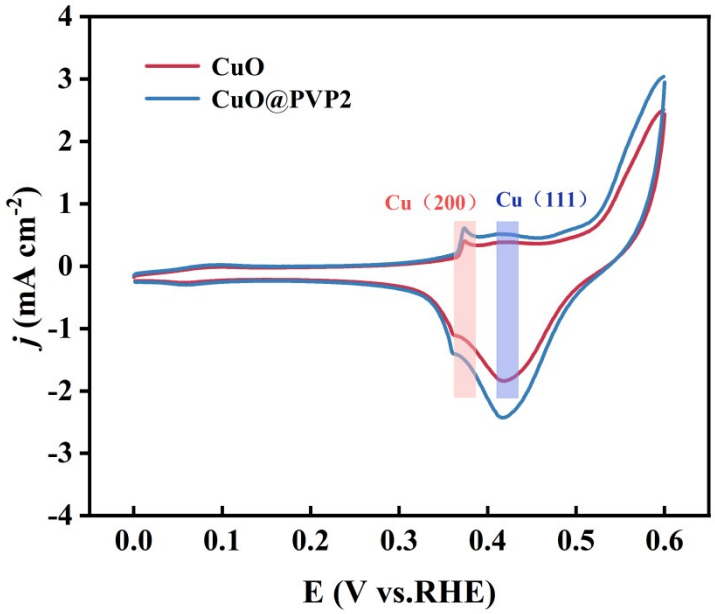

Figure S18. CV curves over CuO and CuO@PVP2 catalysts in 1 M KOH.

Table S1. The performance comparison of this work with the state-of-the-art results.

Catalysts	FE_{C2H4}(%)	FE_{C2+}(%)	References
CuO@PVP	46.7	72.8	This work
Cu-N_2O_2	25	/	[1]
Act-Si-2-Cu-N_4	41.94	/	[2]
CuO	26	44.6	[3]
Cu@[BPy]BF_4-2.4	30.91	/	[4]
CeO_2-CuO	42.3	/	[5]
Cu_2O@Ag-45	/	55.4	[6]
BIC-145	28	/	[7]
Ag-MOF/CuO	45.72	/	[8]

Table S2. EIS equivalent circuit simulation results.

Sample	R_s	R_{ct}
CuO	97.34	67.17
CuO@PVP2	88.7	38.48

Reference

[1] Q. Geng, L. Fan, H. Chen, C. Zhang, Z. Xu, Y. Tian, C. Yu, L. Kang, Y. Yamauchi, C. Li, Revolutionizing CO_2 electrolysis: fluent gas transportation within hydrophobic porous Cu_2O, *J. Am. Chem. Soc*., 2024, **146**, 10599-10607.

[2] Y. Jiang, X. Wang, D. Duan, C. He, J. Ma, W. Zhang, H. Liu, R. Long, Z. Li, T. Kong, Structural reconstruction of Cu_2O superparticles toward electrocatalytic CO_2 reduction with high C_{2+} products selectivity, *Adv. Sci*., 2022, **9**, 2105292.

[3] C. Li, T. Zhang, H. Liu, Z. Guo, Z. Liu, H. Shi, J. Cui, H. Li, H. Li, C. Li, Steering CO_2 electroreduction to C_{2+} products via enhancing localized *CO coverage and local pressure in conical cavity, *Adv. Mater*., 2024, **26**, 2312204.

[4] J. Heng, H. Zhu, Z. Zhao, P. Liao, X. Chen, Fabrication of ultrahigh-loading dual copper sites in nitrogen-doped porous carbons boosting electroreduction of CO_2 to C_2H_4 under neutral conditions, *Adv. Mater*., 2024, **37**, 2415101.

[5] Y. Li, X. Zhang, X. Tai, X. Yang, P. Yu, S. Dong, L. Chi, Z. Wu, Y. Zhang, S. Sun, Highly tension-strained copper concentrates diluted cations for selective proton-exchange membrane CO_2 electrolysis, *Angew. Chem. Int. Ed*., 2025, **64**, e202422054.

[6] Z. Cao, Z. Chen, H. Sun, S. Yao, Z. Liu, F. Li, X. Yang, W. Zhou, J. Fan, H. Wang, Shielding effect in the synthesis of Gd-doped copper oxide catalysts with enhanced CO_2 electroreduction to ethylene, *J. Mater. Chem. A*, 2024, **12**, 29165-29173.

[7] Y. Zhao, Y. Wang, Z. Yu, C. Song, J. Wang, H. Huang, L. Meng, M. Liu, L. Liu, Gold single atom doped defective nanoporous copper octahedrons for electrocatalytic reduction of carbon dioxide to ethylene, *ACS nano.,* 2025, 19, 4505-4514.

[8] T. Yang, Y. Zhang, Z. Huang, J. Yang, M. Kuang, Customized CO_2 electroreduction to methane or ethylene by manipulating *H and *CO adsorption on Cu/CeO_X catalysts, *J. Mater. Chem. A.*, 2024, **12**, 20115-20120.